
# Pyrolyzed chitosan-based materials for $CO_2/CH_4$ separation

Mirtha A.O. Lourenço, Cláudia Nunes, José R.B. Gomes, João Pires, Moisés L. Pinto, Paula Ferreira

PII: S1385-8947(18)32666-4
DOI: https://doi.org/10.1016/j.cej.2018.12.180
Reference: CEJ 20720

To appear in: *Chemical Engineering Journal*

Received Date: 23 October 2018
Revised Date: 30 December 2018
Accepted Date: 31 December 2018

Please cite this article as: M.A.O. Lourenço, C. Nunes, J.R.B. Gomes, J. Pires, M.L. Pinto, P. Ferreira, Pyrolyzed chitosan-based materials for $CO_2/CH_4$ separation, *Chemical Engineering Journal* (2018), doi: https://doi.org/10.1016/j.cej.2018.12.180

# Pyrolyzed chitosan-based materials for $CO_2/CH_4$ separation

*Mirtha A. O. Lourenço,[a*] Cláudia Nunes,[a] José R. B. Gomes,[b] João Pires,[c] Moisés L. Pinto,[d*] Paula Ferreira[a,*]*

[a]CICECO, Department of Materials and Ceramic Engineering, University of Aveiro, Campus Universitário de Santiago, 3810-193 Aveiro, Portugal.

[b]CICECO, Department of Chemistry, University of Aveiro, Campus Universitário de Santiago, 3810-193 Aveiro, Portugal.

[c]CQB and CQE – Center of Chemistry and Biochemistry and Center of Structural Chemistry, Department of Chemistry and Biochemistry, Faculty of Sciences, University of Lisbon, C8, 1749-016 Campo Grande, Lisbon, Portugal.

[d]CERENA, Department of Chemical Engineering, Instituto Superior Técnico, University of Lisbon, Av. Rovisco Pais, n°1, 1049-001 Lisboa, Portugal

*Corresponding Authors

Phone: +351 234 401419; fax: +351 234 401470;

*E-mail addresses: mirtha@ua.pt (M. Lourenço); moises.pinto@tecnico.ulisboa.pt (M. Pinto); pcferreira@ua.pt (P. Ferreira)*

**Keywords**

Adsorption, Chitosan, Periodic mesoporous organosilicas, Pyrolysis, $CO_2/CH_4$ separation.

**Nomenclature**

$C_{18}$-TMA- octadecyltrimethylammonium bromide

DFT- density functional theory

IAST- Ideal Adsorbed Solution Theory

MAC- microwave activated carbon

MOF- metal organic frameworks

PMO- periodic mesoporous organosilicas

$S_{BET}$- specific surface area

VSA- vacuum swing adsorption process

ZIF- zeolitic imidazolate frameworks

$C_1$- First Virial coefficient

$C_2$- Second Virial coefficient

$K$- Henry's constant

$n^{ads}$- amount of gas adsorbed

$p$- pressure

$P/P_0$- relative pressure

$y_{CH_4}$- molar fractions of methane in the gas phases

$x_{CH_4}$- molar fractions of methane in the adsorbed phases

**Abstract**

Chitosan is a biopolymer obtained by deacetylation of chitin extracted from sub-products of the food industry and it is rich and nitrogen content. Pyrolyzed chitosan- and chitosan-periodic mesoporous organosilica (PMO)- based porous materials with different pore structures and chemical features are prepared using different dry methods and ensuing pyrolysis at 800 °C, for application in the $CO_2/CH_4$ adsorption/separation. The highest $CO_2$ adsorption capacity (1.37 $mol \cdot kg^{-1}$ at 100 kPa; 1.9 $mol \cdot kg^{-1}$ at 500 kPa) and the best selectivity for $CO_2/CH_4$ separation (95 at 500 kPa) is obtained using 1.5% (m/v) of chitosan

solution dried under supercritical $CO_2$. This material combines a good $CO_2$ adsorption capacity with one of the highest selectivities for $CO_2/CH_4$ separation of the literature, arising as a promising alternative adsorbent for natural gas or biogas upgrading at reduced cost. The presence of high N content together with pores of diameter around 2 nm leads to an increase of the $CO_2$ adsorption capacity. In the case of chitosan-PMO-based materials, the activation step using both acid and crushing methods is crucial to increase the $CO_2$ adsorbed amount. Here, the highest $CO_2$ adsorption capacity and the highest selectivity are obtained by the chitosan-PMO crushed adsorbent and the chitosan-PMO material activated with sulfuric acid, respectively. These observations indicate the importance of the controlled attack of the material surface to enhance the diffusion of the target gases within the adsorbent, avoiding the adsorption of other species.

## 1. Introduction

Biogas is a clean and renewable form of energy thought as an alternative to fossil fuels. It is obtained by anaerobic digestion process of organic matter (sewage, animal byproducts, and agricultural, industrial and municipal solid waste).[1–8] It is a mixture of gases mostly composed by methane ($CH_4$, 60 - 70 %) and carbon dioxide ($CO_2$, 30 - 40 %) and traces of other gases such as $H_2S$, CO, $H_2$ or $N_2$. The methane fraction of biogas has a huge interest for household applications, fuel vehicles or electricity generation. Thus, an efficient methodology to separate methane from carbon dioxide is needed.[1] Nowadays, the removal of $CO_2$ from $CH_4$ is mainly made using absorption processes, employing amine solvents (monoethanol amine, diethanolamine or methyl diethanolamine), which chemically interact with $CO_2$. However, these amine solvents show several disadvantages namely: low $CO_2$ capacity; degradation of the amine solvent in contact with $NO_x$, $SO_x$, $O_2$

gases; high cost of solution regeneration; corrosion of the equipment by the amine solvent; and lastly, scale up difficulties.[9] Thus, efforts are being made to prepare efficient and regenerable solid adsorbents to uptake the $CO_2$ contaminant from $CH_4$, turning biogas applicable in a wide range of applications, and also to prevent the corrosion of equipment and pipelines promoted by the acid $CO_2$ gas.[10,11] The ideal adsorbent needs to exhibit high capacity, perfect selectivity, long-term durability, thermal and chemical stability, fast uptake processes, easy regeneration consistent with negligible capacity loss on multiple adsorption/desorption cycles, and low cost.[12] Additionally, since this application targets large scale industrial processes which require large amounts of the adsorbent, the materials should be prepared from sustainable resources.

Affordable materials, such as activated carbons, continue to attract attention for $CO_2$ removal from many systems as they are reversible $CO_2$ adsorbents and present high adsorption capacity per mass unit.[13–18] However, these materials usually present low selectivity in the $CO_2/CH_4$ adsorption/separation.[16,18] To prepare efficient adsorbents for $CO_2/CH_4$ adsorption-separation, the materials must hold high specific surface areas and microporosity. It was observed that the presence of nitrogen in metal organic frameworks (MOF)[19,20], activated carbons[21], periodic mesoporous organosilicas[20,22,23] and organic modified silicas[20,24,25] enables the enhancement of the separation selectivity. Nevertheless, most of these materials are expensive and have several drawbacks that hamper their application in realistic scenarios.[20]

Chitosan is a widely available polysaccharide obtained from biomass wastes with high nitrogen content and thus has been considered for $CO_2$ capture. Some authors explored this polymer with crystalline domains dissolved in the ionic liquid (IL) [Bmim]Cl to afford chitosan-IL solutions for $CO_2$ capture and storage applications.[26–28] Both pure IL and

pure chitosan show low $CO_2$ absorption abilities, but 10 wt% chitosan/IL solution displays almost 8.1% $CO_2$ fixing efficiency. Recently, Qaroush et al.[29] also reported the use of chitosan hydrochloride oligosaccharide dissolved in dimethyl sulfoxide (DMSO) as a suitable absorbent for $CO_2$ capture. Despite these promising results, the adsorption technology employing solid adsorbents is usually associated to operation costs that are lower than those occurring for the absorption strategy and looks, therefore, very appealing. Thus, several authors investigated the potential of chitosan, in the form of pyrolyzed spheres, to capture $CO_2$. Primo *et al.*[30] demonstrated that pyrolyzed chitosan beads display similar $CO_2$ adsorption when compared with the most efficient active carbons and double adsorption capacity at low relative pressures, due to the presence of *N*-doping elements. However, the authors[30] only tested the material in the $CO_2$ adsorption at low temperature (0 °C) and it is well known that the increase of the adsorption temperature negatively affects the performance of the adsorbents regarding the adsorption capacity and selectivity. Thus, improvements should be made in the adsorbents so they can operate under the conditions of the biogas upgrading.

The pore size/geometry and polarity of the material are also key features to achieve selective adsorbents as it was recently discussed in the review paper of Oschatz *et al.*[31] For example, it was observed that the pore size and pore curvature of the PMO sorbents directly influenced the diffusion of the reagents or gas molecules inside the pores.[20,22,23,32] These materials are already potential candidates for the $CO_2/CH_4$ separation as previously reported.[20]

To the best of our knowledge we describe for the first time the preparation of chitosan particles by different drying strategies (i) at room temperature, ii) at 40 °C in conventional oven and iii) under supercritical $CO_2$) followed by pyrolysis under nitrogen atmosphere in a

comprehensive study. Additionally, in an attempt to enhance porosity and surface area, pyrolyzed chitosan-PMO composites (as-made and surface attacked with $H_2SO_4$) are also prepared and studied. $CO_2$ and $CH_4$ adsorption isotherms are studied in all materials, at pressures up to 1000 kPa, to assess their potential for the separation of these two gases in a mixture and correlated with the physicochemical characterization (specific surface area, pore volume, pore diameter, accessibility and nitrogen content), to fully understand its relationship with the $CO_2/CH_4$ separation ability for biogas upgrading.

## 2. Experimental section

### 2.1. Chemicals and Reagents

Octadecyltrimethylammonium bromide ($C_{18}$-TMA, 98%, Aldrich), sodium hydroxide (NaOH, 100%, eka), ethanol (99.9%, Riedel-de Haën), hydrochloric acid (HCl, 37% v/v, Carlo Erba), Chitosan (medium weight, Aldrich), acetic acid ($CH_3COOH$, Sigma-Aldrich), sulfuric acid ($H_2SO_4$, 95-97% v/v, PanReac), Ammonium sulfate ($(NH_4)_2SO_4$, 99%, Panreac) were purchased from commercial sources. All chemicals are used as received. 1,4-bis(triethoxysilyl)benzene (BTEB)[33] is prepared *via* a Grignard reaction, followed by distillation in vacuum.

### 2.2. Materials synthesis

#### 2.2.1. Ph-PMO material preparation

Phenylene-bridged PMO was prepared following procedures previously described in the literature.[34,35] In a typical synthesis of the Ph-PMO material, the $C_{18}$-TMA is dissolved in a mixture of distilled water and 6 M aqueous sodium hydroxide at 20 – 60 °C. BTEB is then added dropwise under vigorous stirring, at room temperature. The molar ratio BTEB:

water : surfactant : NaOH is always constant and equal to 1 : 531 : 0.96 : 4.05. The mixture is ultra-sonicated during 20 min at room temperature (Bransonic ultrasonic cleaner 1510E-DTH). The reaction mixture is stirred for 24 h at room temperature, and is subsequently moved into a Teflon lined autoclave for another 24 h at 100 °C. The final white precipitate is recovered by filtration, washed with warm distilled water and dried at 60 °C. The surfactant is removed employing a typical solvent extraction approach, using EtOH/HCl solution.[34–38] The powder is filtered off, washed with ethanol and water and dried overnight at 60 °C.

### 2.2.2. Chitosan spheres preparation

Chitosan spheres are prepared using a literature modified procedure previously described by Primo *et al.* [30]. An acidic solution of 1.5% (w/v) of chitosan (1 g chitosan in 67 mL of a 0.1 M $CH_3COOH$ aqueous solution)[39] is dropped into an aqueous basic solution (4 M, NaOH). A chitosan alcogel is consequently obtained by sequentially introducing the hydrogel beads in a series of ethanol/water solutions of increasing alcohol concentration (10, 30, 50, 70, 90 and 100% v/v) for 15 min each. The chitosan alcogel beads are then dried using different methodologies: i) dried at room temperature for 30 days; ii) dried in an oven at 40 °C during 24 h and iii) dried in supercritical $CO_2$ ($supCO_2$) at above $73 \times 10^{-2}$ $kPa^{-1}$ and 31 °C, using a E3000 critical point drying apparatus for 4 h, to give chitosan aerogel beads denoted as: Chit_air; Chit_40°C and Chit_$supCO_2$, respectively. All these different spheres are introduced into a saturated $(NH_4)_2SO_4$ solution for 1 h. After recovery from the solution, the wet spheres are pyrolyzed under nitrogen atmosphere as described in section 2.2.4 - “Pyrolysis of chitosan-based materials”. A schematic representation of the synthesis procedure can be found in Figure S1a.

### 2.2.3. Chitosan-PMO composite particles preparation

Ph-PMO (200 mg) is added to an acidic solution of chitosan (1 g chitosan in 25 mL of a 0.3 M $CH_3COOH$ aqueous solution) and stirred overnight. The chitosan solution is modified relatively to the pure chitosan spheres in order to reduce the viscosity of the solution and to allow a homogeneous mixture with the PMO. The resulting mixture is dropped into aqueous basic solution (NaOH, 4 M). A chitosan-PMO alcogel is obtained after switching water with ethanol as specified above. The chitosan-PMO alcogel beads are dried in supercritical $CO_2$, resulting in chitosan-PMO composite aerogel spheres (named Chit-PMO). After treating these beads in a saturated $(NH_4)_2SO_4$ solution for 1 h, the wet beads are recovered for further pyrolysis treatment (cf. section 2.2.4. "Pyrolysis of chitosan-based materials"). A schematic representation of the synthesis procedure can be found in Figure S1a.

### 2.2.4. Pyrolysis of chitosan-based materials

The prepared chitosan-based materials are pyrolyzed in an alumina crucible at 800 °C under nitrogen atmosphere. The pyrolysis is performed in two steps. Initially, annealing was carried out at 200 °C for 2 h using a heating rate of 5 °C·min$^{-1}$. Then, the temperature is dropped down at 35 °C. Subsequently, using the same heating rate, the temperature is increased till it reached 800 °C, and it is maintained at this value for further 2 h. Natural cooling to room temperature is made under nitrogen flow. After pyrolysis, the samples are denoted as Chit_air_P800; Chit_40°C_P800, Chit_sup$CO_2$_P800 and Chit-PMO_P800.

### 2.2.5. Surface opening procedure

To increase the accessibility of the gaseous molecules into the pyrolyzed chitosan-PMO-based material two different procedures are performed:

i) acid chemical post-treatment: the particles of Chit-PMO_P800 are heated with $H_2SO_4$ at 160 °C during 6 h, cooled to room temperature and then pyrolyzed at 800 °C to obtain the Chit-PMO_P800/$H_2SO_4$_P800 material.

ii) Crushing: The particles of both Chit-PMO_P800 and Chit-PMO_P800/$H_2SO_4$_P800 materials are crushed smoothly using a mortar and pestle, without grinding the material spheres.

A schematic representation of the synthesis procedure can be found in Figure S1b.

## 2.3. Materials characterization

The chitosan-based materials are evaluated by -196 °C $N_2$-sorption isotherms, scanning electron microscopy (SEM), elemental analysis (EA), Fourier transformed infrared (FTIR), Raman spectroscopies and thermogravimetric analyses (TGA). More information concerning the measurements (specific methods, equipment models and conditions used) is available in the supplementary material (SM).

## 2.4. High pressure $CO_2$ and $CH_4$ adsorption

Adsorption isotherms of carbon dioxide and methane are measured on the chitosan-based materials, at 25 °C and pressures up to 1000 kPa, using the volumetric method. Reproducibility of the measurements is better than ±2.5% in the amounts adsorbed. The

samples are degassed at 150 °C during 2.5 h under vacuum of $10^{-6}$ hPa. The $CO_2$ and $CH_4$ gases are used as provided by Air Liquide (France), with a purity of 99.998% and 99.95%, respectively.

The gas adsorption is measured on a lab made stainless steel volumetric apparatus, with a pressure transducer (MKS, Baratron 627D14TBC). A stirred thermostatic water bath (Julabo, MB) is used to control the temperature of the sample and of the adsorption system. The non-ideality of the gas phase is considered by the use of the second and third virial coefficients. Moreover, the experimental excess adsorbed amounts are converted to the absolute adsorbed amounts having into account the pore volume of each sample and the density of the gas phase using the virial coefficients. Each experimental pure component adsorption isotherm is fitted using the Virial model. Selectivity values are estimated using a method proposed by Myers[40] and the implementation is described in detail in previous works[41,42].

## 3. Results and Discussion

### 3.1. Characterization of Materials

The porosity and structural order of the pyrolyzed chitosan-based materials are studied by $N_2$ adsorption/desorption isotherms and SEM. Figure 1 shows the $N_2$ sorption isotherms of pyrolyzed Chit and Chit-PMO based samples, respectively, and Table 1 summarizes the textural features of the samples. The presence of different micro- and meso- pores is confirmed by low temperature (-196 °C) $N_2$ adsorption–desorption experiments. In Figure 1 is possible to observe that the samples display different type of curves. Pyrolyzed chitosan and chitosan-PMO based materials dried with supercritical $CO_2$ (Figure 1a), at 40 °C in an

oven (Figure 1b) or at ambient air (Figure 1c) present a Type II curve (IUPAC classification)[43], usually observed for nonporous or macroporous materials. However, the crushing of the beads of pyrolyzed Chit-PMO samples revealed a Type IV curve, which is typical of conventional mesoporous materials such as MCM-41[44], indicating the remaining of the characteristic mesoporosity of the PMO material.

As it can be seen in Table 1, the specific surface area ($S_{BET}$) of the particles of the pyrolyzed chitosan-based materials is very small. This happens probably because the external surface of the pyrolyzed chitosan-based particles is very compact and the $N_2$ can only diffuse to the interior of the material through the narrow micropores, which corresponds to a very slow process at -196 °C. When the particles of pyrolyzed Chit-PMO-based materials are crushed, accessibility of the pores to nitrogen at the interior of the beads at -196 °C increases and the $S_{BET}$ increased significantly. The maximum intensities of the pore size distributions for all the materials are ≈1.5 nm with the exception of Chit_sup$CO_2$_P800 (Table 1). The minimal surface area observed in the evaporative drying processes can be also explained by the tension of the meniscus at the solvent–vapor interface that draws together the colloidal units of the gel, promoting shrinkage and cracking of the structure.[45] Note that in previous works the best results in the preservation of the materials structure was obtained by employing supercritical $CO_2$ drying due to the absence of surface tension of the supercritical $CO_2$.[45,46] Moreover, the use of this method to dry polymers usually leads to the formation of a structure with micro-, meso- and macro- pores.[45]

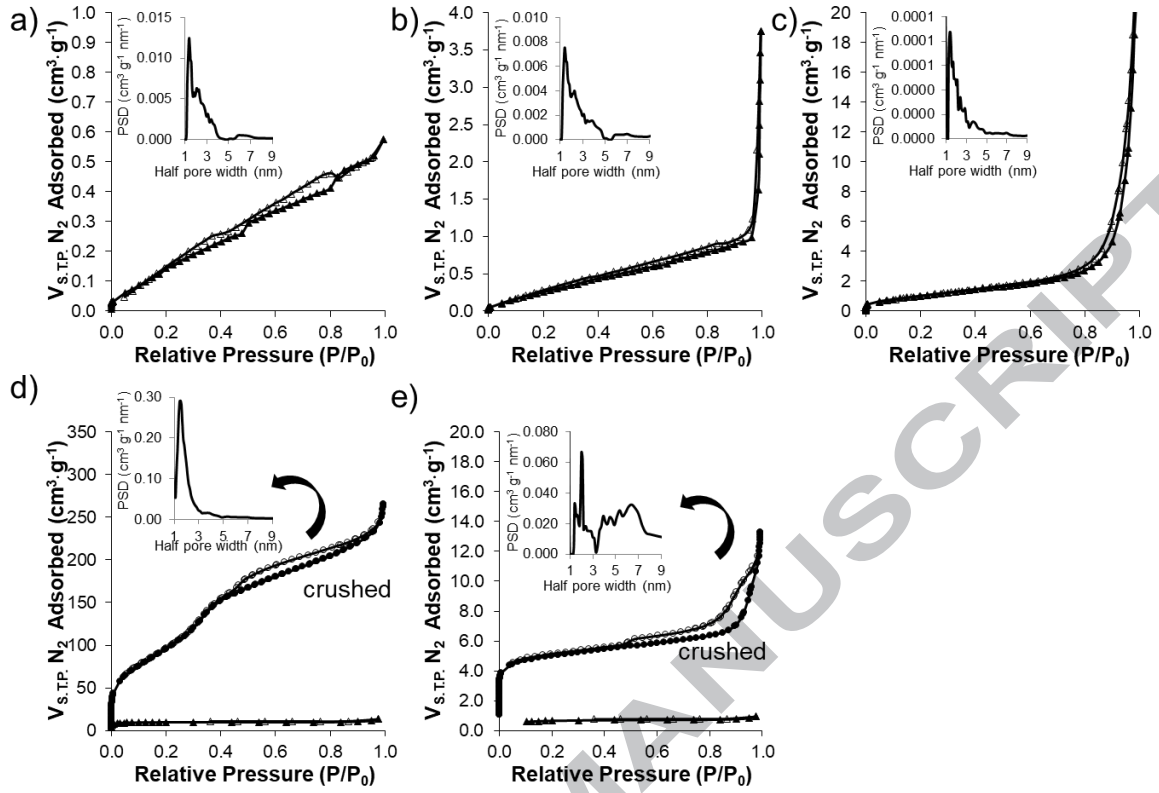


**Figure 1.** $N_2$ adsorption-desorption isotherms, at -196 °C, of a) Chit_sup$CO_2$_P800, b) Chit_40°C_P800, c) Chit_air_P800, d) Chit-PMO_P800 and e) Chit-PMO_P800/$H_2SO_4$_P800 (circles correspond to the crushed composite materials, filled symbols correspond to adsorption process, empty symbols correspond to desorption process). The insets show the pore size distribution (PSD) curves of the materials determined by the DFT method.

**Table 1.** Textural properties of pyrolyzed Chit and pyrolyzed Chit-PMO based materials.

| Sample | $S_{BET}$ / $m^2 \cdot g^{-1}$ | $V_P$ / $cm^3 \cdot g^{-1}$ [a] | $d_P$ / nm [b] | Curve type |
|---|---|---|---|---|
| Chit_air_P800 | 9 | 0.008 | 1.49 | II |
| Chit_40°C_P800 | 10 | 0.014 | 1.49 | II |
| Chit_sup$CO_2$_P800 | 15 | 0.015 | 1.97 | II |
| Chit-PMO_P800 | 34 | 0.015 | - | II |
| Chit-PMO_P800/$H_2SO_4$_P800 | 2 | 0.001 | - | II |
| Chit-PMO_P800_crushed | 376 | 0.346 | 1.51 | IV |
| Chit-PMO_P800/$H_2SO_4$_P800_crushed | 325 | 0.327 | 1.49 | II |

[a]Pore volume determined by DFT method. [b]Pore radius obtained from the BJH method calculated on the basis of adsorption data.

SEM micrographs, in Figure 2, show the morphologic characteristics of the pyrolyzed chitosan–based materials. Chit_sup$CO_2$_P800 material presents a rough surface (Figure 2a) with evident signs of macroporosity (Figure 2a - inset). The drying with supercritical $CO_2$ seems to generate sponge type structures. Chit_40°C_P800 particles show a smooth surface, almost without porosity (Figure 2b). The inner regions of the particles seem to be denser than the ones of the former material and display some macroporosity (Figure 2b - inset) and cracks (Figure 2b). The drying in air of the chitosan spheres (Chit_air_P800) led to dense aggregates of particles (Figure 2c). All these results are in agreement with the Type II isotherm observed in the $N_2$-sorption isotherms measurements. In the case of the Chit-PMO_P800 based materials (Figure 2d-e), it is possible to observe the PMO particles dispersed inside the macroporous chitosan polymer (Figure S2, SM). The Chit-PMO_P800/$H_2SO_4$_P800 material shows also a quite rough chitosan polymer surface (Figure 2e) when compared with the Chit-PMO_P800 material (Figure 2d), a consequence of the surface attack with sulfuric acid.

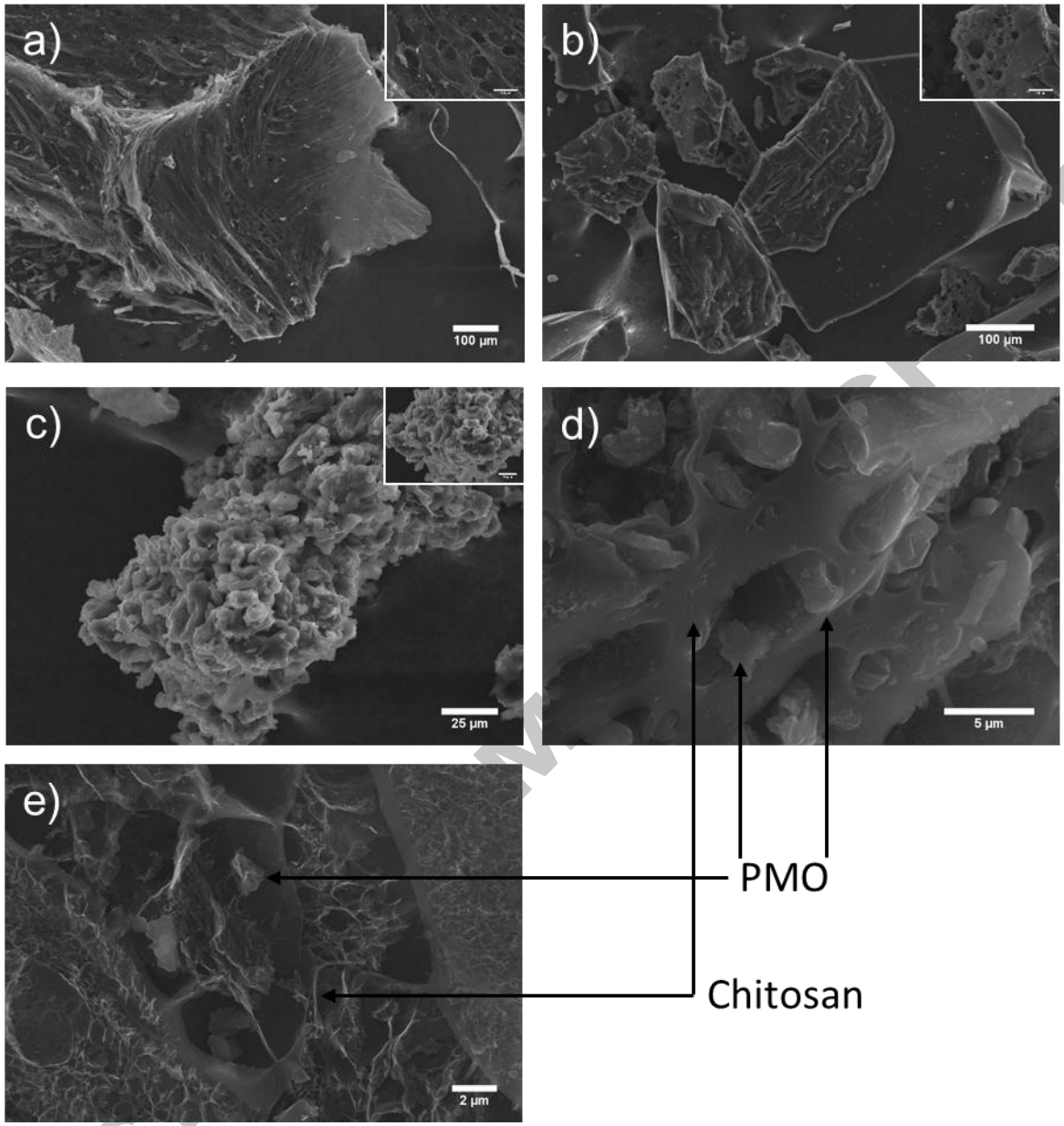


**Figure 2.** SEM images of crushed samples of a) Chit_sup$CO_2$_P800, b) Chit_40°C_P800, c) Chit_air_P800, d) Chit-PMO_P800 and e) Chit-PMO_P800/$H_2SO_4$_P800.

The chemical functional groups present in the pyrolyzed chitosan- and chitosan-PMO-based materials are verified by Fourier infrared transform (FTIR) spectroscopy, Figure S3 (SM). The FTIR spectra of the pyrolyzed Chit- and Chit-PMO-based materials display a wide band between 3350-3450 $cm^{-1}$ that can be endorsed to either OH stretching or NH

stretching vibration, indicating the presence of hydroxyl and amino groups, respectively.[47,48] Also, the peaks at 1075-1120 $cm^{-1}$ and 1550-1668 $cm^{-1}$ can be endorsed to C-N stretching vibrations and N-H bending, respectively, and are presented in all the materials considered. The peaks corresponding to the C-N stretching vibration are less visible in the Chit_air_P800 sample. Chit_sup$CO_2$_P800 and Chit_40°C_P800 exhibited several peaks in the range of 1360−1530 $cm^{-1}$, which can be assigned to the stretching modes of C−N heterocycles for pyridine and pyridinium species, as observed by Primo *et al*. upon XPS analysis.[30] Moreover, the band at 630-700 $cm^{-1}$ can be related to NH wagging vibration. The bands corresponding to the Si−O−Si stretching vibrations and bending of Si–O–Si of the phenylene-PMO appear at 1095-1110 and *ca*. 615 $cm^{-1}$, respectively,[49] which is supported by the increase of their intensity on going from the bare chitosan to the PMO containing samples. The overtones of benzene ring vibrations are also observed between 1300–1750 $cm^{-1}$. The small shoulder between 2913-2956 $cm^{-1}$ can be related to symmetric stretching vibration of the C−H bond that can be attributed to the presence of aliphatic groups.[48] The materials show the presence of alcohol groups, as supported by the presence of its characteristic vibrational modes such as deformation of OH bond, above 1425 $cm^{-1}$ and 1350 $cm^{-1}$, stretching of C-O bond at 1095-1110 $cm^{-1}$ as well as at 1045 $cm^{-1}$.[50] The spectrum of the pyrolyzed chitosan-PMO sample treated with sulfuric acid shows a band at 1686 $cm^{-1}$, which is assigned to the stretching of C=O bond, indicating the presence of carbonyl groups.[48]

The Raman spectra of the prepared materials are depicted in Figure S4, and suggest the presence in all samples of graphitic carbons with high tendency to become crystalline. Although, the drying method of the chitosan spheres influences the crystallization degree of the graphitic carbons. The crystallization degree of graphitic carbon in the chitosan

particles seems to increase in the following way: Chit_sup$CO_2$_P800 < Chit_40°C_P800 < Chit_air_P800, evidenced by the increase of intensity and degree of definition of the peaks observed at *ca.* 1315 and 1570 $cm^{-1}$. The material dried slowly (under air, at 25 ºC for 30 days) presents the highest graphitization degree. The Raman spectra of both pyrolyzed chitosan and chitosan-PMO-based materials showed the maximum peaks of the G and D bands between 1550 and 1591 and 1308 and 1331 $cm^{-1}$, respectively (Figure S4). Both G and D bands are typically observed in carbonaceous materials, including graphite and carbon nanotubes, and can be attributed to stretching vibrations of aromatic rings and defects, respectively.[51,52]

Table S1 (SM) shows the N content into the pyrolyzed chitosan and pyrolyzed chitosan-PMO -based materials determined by elemental analysis results. The presence of high amount of N on the materials (between 7 and 13%) indicates that the N groups of chitosan are still incorporated in the structure of the pyrolyzed chitosan-based materials. The material with the highest N content is the Chit_sup$CO_2$_P800 (12.94%), followed by Chit_40°C_P800 (9.38%) and Chit-PMO_P800 materials (between 7 and 7.5% of N). The low C and N percentage observed in the Chit-PMO based materials is explained by the addition of PMO with large content of silicon and oxygen elements. Additionally, the materials dried with supercritical $CO_2$ or at 40 °C have some S content that can be related with the ability of these materials to adsorb $SO_4^{2-}$ species from $(NH_4)_2SO_4$ solution. This ability seems to be superior for the chitosan-based materials dried with supercritical $CO_2$. The material displaying the lowest w/w percentage of C (11.56%) and N (< 0.5%) is the Chit_air. This occurs because of the extreme thermal stability of the material which cannot be burn up to 1075 °C (the temperature of operation of the elemental analysis equipment). Note that this sample is highly compact as observed by SEM (Figure 2c) and also presents

highly graphitic level as seen in the RAMAN spectrum (Figure S4). These results indicate that the utilization of supercritical $CO_2$ drying strategy seems to be beneficial in terms of preserving the nitrogen content into the pyrolyzed chitosan beads and, thus, can be associated with the ability to remove the solvent from chitosan spheres (in a shorter time and at a lower temperature than those used with the other drying strategies considered here) without promoting any amine degradation.

Figure 3 shows the XPS spectra of the samples Chit_sup$CO_2$_P800 and Chit_air_P800. Both samples have C, O, N and Na species (Figure 3a-b). The presence of Na species can be related with the NaOH solution used to precipitate the chitosan particles. The amount of Na in the Chit_sup$CO_2$_P800 sample seems to be lower than in the Chit_air_P800, which can be explained by the Na leaching away from the material by action of the supercritical $CO_2$ fluid, during the drying process. The N content is very low in the Chit_air_P800 material. This can be explained by the degradation and release of the amino groups during the drying step before and during pyrolysis. The high-resolution spectra (N 1s) revealed the form of nitrogen in the carbon matrix.

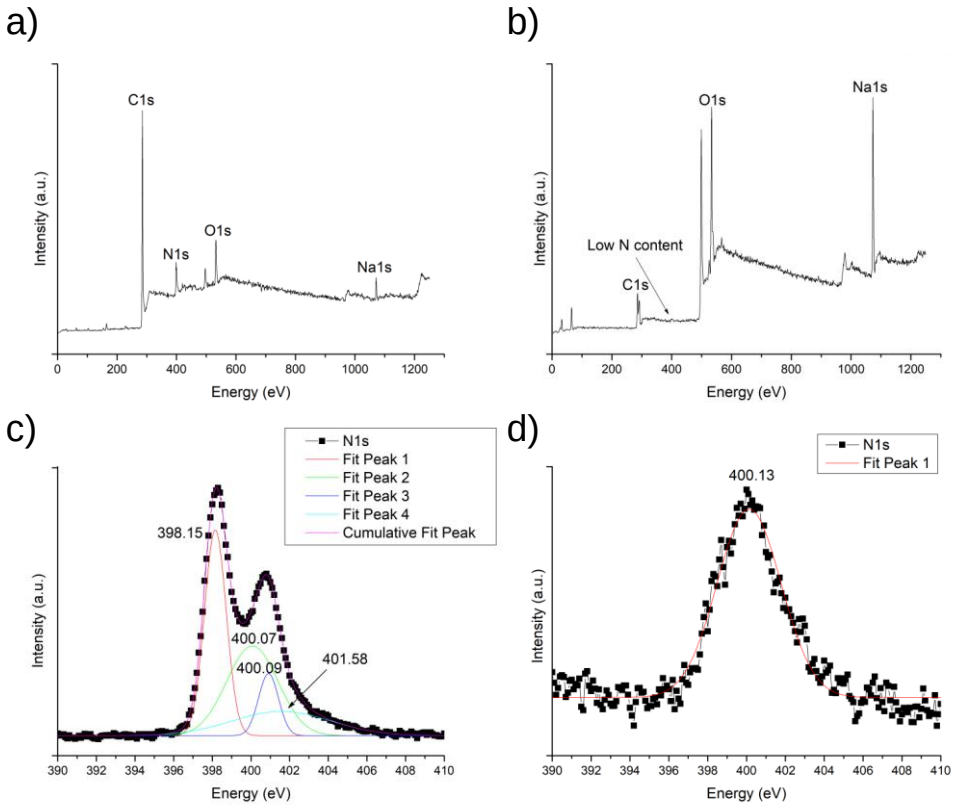


**Figure 3.** XPS survey spectra of a) Chit_sup$CO_2$_P800 and b) Chit_air_P800 samples; and N 1s peak of c) Chit_sup$CO_2$_P800 and d) Chit_air_P800 samples.

The N 1s deconvoluted spectrum for the Chit_sup$CO_2$_P800 material have 4 binding energies, one at 398.2 ± 0.4 eV, two at ~400.1 eV, and another at around 401.6 eV, corresponding to pyridinic, pyrrolic, and/or pyridone-type nitrogen, and quaternary nitrogen respectively.[30,53] In the case of the chit_air only a single peak is observed at 400.13 eV and it is assigned to the presence of pyrrolic and/or pyridone-type nitrogen species.

Figure S5 (SM) shows the TGA analyses of pyrolyzed chitosan and pyrolyzed chitosan-PMO based materials up to 800 °C. The weight loss observed below 150 °C is related to desorption of physisorbed water for all adsorbents. Differences in the chemical stability of the materials are observed by varying the drying method. The Chit_sup$CO_2$_P800 shows a

second weight loss (≈10%) between 200 and 400 °C that can be related with the loss of the amine and hydroxyl groups followed by a two-step degradation and release of the remaining organic groups at temperatures above 400 and 600 °C. These probably occur due to the presence of different degrees of graphitization. In the case of Chit_40°C_P800 and in both pyrolyzed chitosan-PMO-based materials, the decomposition and release of the organic groups of chitosan initiate at *ca.* 400 °C. In the latter materials the decomposition and release of the phenylene-moieties of the PMO start above 550 °C. The Chit_air_P800 material shows a 2% mass loss between 270 and 500 °C. This material presents the highest thermal stability of all pure chitosan materials, presenting less than 5% weight loss between 100 and 800 °C. Figure S5f shows the TGA/DTA of the Chit_air_P800 material up to 1200 °C. It is possible to observe that between 120 and 1075 °C only 15% of the weight is lost. The presence of Na is also evidenced by the TGA analysis and corresponds to the 1% weight loss at approximately 890 °C (the boiling point of Na is 882.8 °C). A 20% mass loss is observed between 1075 and 1200 °C. This loss is attributed to the graphitic carbon (observed by Raman spectroscopy, Figure S4) decomposition. Note that graphitic carbon is thermally stable up to 900 °C similarly to diamond.[54]

### 3.2. Experimental pure-component adsorption isotherms

Pure $CO_2$ and $CH_4$ adsorption isotherms measured at 25 ºC on the pyrolyzed chitosan and chitosan-PMO -based materials are displayed in Figure 4. As it can be observed the drying method has a huge influence on the adsorption of $CO_2$ and $CH_4$ and, also, on the separation of these gases.

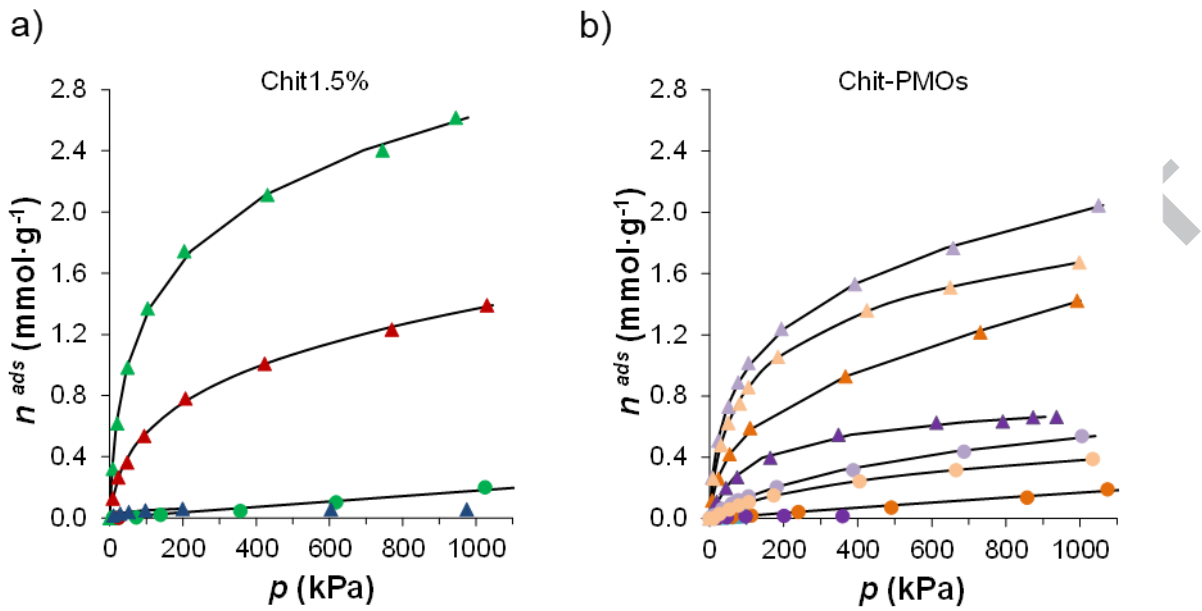


**Figure 4.** Adsorption equilibrium isotherms of pure $CO_2$ (triangle symbols) and $CH_4$ (circle symbols) gases at 25 ºC in the a) pyrolyzed Chit based samples (green - Chit_sup$CO_2$_P800, red - Chit_40°C_P800, blue - Chit_air_P800) and b) pyrolyzed Chit-PMO based materials (dark purple - Chit-PMO_P800, light purple - Chit-PMO_P800_crushed, dark orange - Chit-PMO_P800/$H_2SO_4$_P800 and light orange - Chit-PMO_P800/$H_2SO_4$_P800_crushed). Solid lines represent the fits of the Virial isotherm model.

The pyrolyzed chitosan particles dried under air, at room temperature (blue symbols, Figure 4a) present the lowest adsorption capacity of $CO_2$, while the pyrolyzed chitosan particles dried using the supercritical $CO_2$ method (green symbols, Figure 4a) showed the highest adsorption capacity for this gas. This can be related with the possible presence of nanosized pores in the supercritical $CO_2$ dried sample[46] that together with meso- and macro- pores leads with an improvement in the adsorption capacity for $CO_2$. Additionally, as observed in Figure 2 (SEM images), the use of evaporating drying methods leads with the formation of denser materials which can decrease the diffusion of the $CO_2$ molecules into the material.

Despite the increase of the specific surface area upon the addition of PMO during the formation of the chitosan particles (Table 1), the adsorption capacity values for $CO_2$ displayed by the pyrolyzed Chit-PMOs are inferior to those obtained for the Chit_sup$CO_2$_P800 material (*cf.* Figure 4).

The activation method of the surface in the pyrolyzed chit-PMO-based materials has high impact on the adsorption capacity of the materials. For instance, the addition of $H_2SO_4$ followed by pyrolysis at 800 ºC leads to an increase of the adsorption capacity of the $CO_2$ gas of chit-PMO_P800 material (Chit-PMO_P800/$H_2SO_4$_P800, Figure 4b in purple symbols), but when the particles are crushed, this increase is even more remarkable. The Chit-PMO_P800/$H_2SO_4$_P800_crushed material is the one presenting the highest adsorption capacity for $CO_2$ (Figure 4b). The same tendency is also observed for the adsorption of $CH_4$ (Figure 4b spherical symbols).

All prepared pyrolyzed chitosan-based materials adsorb higher amounts of $CO_2$ than $CH_4$. In fact, for the materials prepared only from chitosan, $CH_4$ adsorption could only be measured in the case of the Chit_sup$CO_2$_P800 sample, because the adsorbed amounts displayed by the other two materials are below the sensitivity of the method.

Having on consideration the low $CH_4$ adsorption capacity obtained for all pyrolyzed chitosan and pyrolyzed chitosan-PMO -based materials, it is possible to generalize that these materials are weak $CH_4$ adsorbents. Table 2 shows the calculated Henry's constants of pure $CO_2$ and $CH_4$ adsorption in the pyrolyzed chitosan and pyrolyzed chitosan-PMO -based adsorbents. Note that the Henry constants for the $CH_4$ adsorption in Chit_40°C_P800 and Chit_air_P800 materials could not be determined because of the negligible adsorbed amounts of the gas in these materials.

The use of supercritical $CO_2$ to dry the samples, and both acid and crushed activation methods provide an enhancement of the adsorption capacity of the pyrolyzed chitosan and pyrolyzed chitosan-PMO -based materials as can be understood from the increase of the Henry's constant for both $CO_2$ and $CH_4$. Overall results indicate that the amount of N species in the materials has high influence in the adsorption of $CO_2$. In fact, despite being the material with the lowest specific surface area (cf. Table 1), Chit_sup$CO_2$_P800 is the material presenting the highest Henry's constant ($7.73 \times 10^{-2}$ mol·kg$^{-1}$·kPa$^{-1}$, Table 2). This can be related with the highest N content among the tested samples (Table S1). The combination of both specific surface area (together with the accessibility to the pores) and amount of nitrogen species in the Chit-PMO_P800_crushed materials leads to the second highest Henry's constant for the $CO_2$.

**Table 2.** Virial coefficients ($C_1$ and $C_2$) and Henry's constants ($K$) for the adsorption of $CH_4$ and $CO_2$ at 25 °C on the prepared materials.[a]

| Gas | Material | $K$ (mol·kg$^{-1}$·kPa$^{-1}$) × $10^{-2}$ | $C_1$ kg·mol$^{-1}$ | $C_2$ (kg·mol$^{-1}$)$^2$ | $CO_2/CH_4$ ratio[b] |
|---|---|---|---|---|---|
| $CH_4$ | Chit_air_P800 | | | | |
| | Chit_40°C_P800 | | | | |
| | Chit_sup$CO_2$_P800 | 0.02 | 0 | | |
| | Chit-PMO_P800 | 0.02 | 0 | | |
| | Chit-PMO_P800/$H_2SO_4$_P800 | 0.02 | 0.49 | | |
| | Chit-PMO_P800_crushed | 0.19 | 2.39 | | |
| | Chit-PMO_P800/$H_2SO_4$_P800_crushed | 0.14 | 3.46 | | |
| $CO_2$ | Chit_air_P800 | 0.19 | 8.32 | 0.04 | - |
| | Chit_40°C_P800 | 2.12 | 2.65 | -0.48 | - |
| | Chit_sup$CO_2$_P800 | 7.73 | 1.35 | -0.03 | 434 |
| | Chit-PMO_P800 | 0.50 | -0.68 | 5.36 | 25 |
| | Chit-PMO_P800/$H_2SO_4$_P800 | 2.93 | 3.59 | -1.03 | 160 |
| | Chit-PMO_P800_crushed | 7.11 | 2.29 | -0.26 | 38 |
| | Chit-PMO_P800/$H_2SO_4$_P800_crushed | 3.46 | 1.56 | 0.15 | 24 |

[a] Obtained by nonlinear least-squares fitting of the virial equation to the adsorption data. [b]Ratio of the Henry's constant for $CO_2$ to that for $CH_4$.

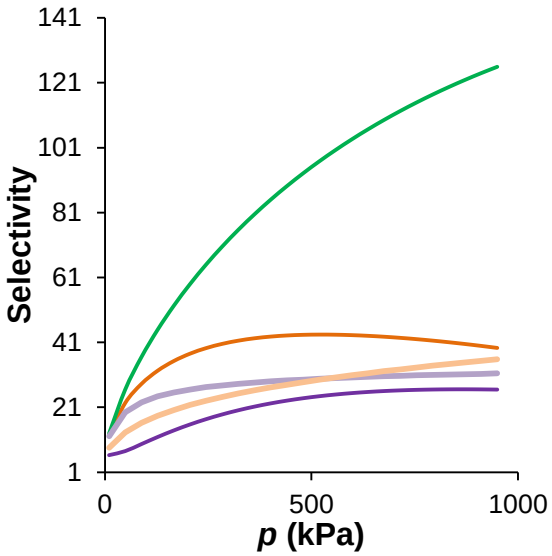


**Figure 5.** Comparative selectivity, at 25 ºC, of Chit_sup$CO_2$_P800 and Chit-PMO_P800 based materials. Scheme color: green - Chit_sup$CO_2$_P800, dark purple - Chit-PMO_P800, light purple - Chit-PMO_P800_crushed, dark orange - Chit-PMO_P800/$H_2SO_4$_P800 and light orange - Chit-PMO_P800/$H_2SO_4$_P800_crushed.

Using the virial equation fitted to the adsorption data and the Ideal Adsorbed Solution Theory (IAST),[55] the selectivity of the separation and the equilibrium phase diagrams for the adsorbed phase can be obtained using a method proposed by Myers[40] with the implementation described in detail in previous works[41,42]. Figure 5 shows that the Chit_sup$CO_2$_P800 is the material with the highest selectivity value (95 at 500 kPa) in the $CO_2/CH_4$ separation. This is probably due to concomitant effect of the presence of high amounts of nitrogen species and of the macroporosity of the surface, which favoured the sorption of $CO_2$ and not that of $CH_4$. In fact, since no significant microporosity is observed with the $N_2$ low temperature adsorption (Table 1), it was assumed that a significant part of the $CO_2$ uptake observed in the sample may be sorbed at the Chit_sup$CO_2$_P800 surface. This material is followed by the Chit-PMO_P800/$H_2SO_4$_P800 (selectivity value of 43 at

500 kPa) adsorbent despite Chit-PMO presents higher Henry's constant for the $CO_2$ than the former material. Both materials present similar N content, thus, this result can be related with the accessibility of the methane molecules to the pores of the materials. The use of acid to activate the Chit-PMO_P800 particles by attacking their surface, potentially allows the penetration of the $CO_2$ species through the materials but not of the $CH_4$. However, the crushed Chit-PMO_P800 samples show significantly higher adsorption capacities than the corresponding non-crushed samples and are in this way more attractive for possible applications.

The influence on the separation can be clarified in Figure 6 where it can be seen the highest performance of Chit_sup$CO_2$_P800 relatively to the other samples. If one considers a gas mixture with 0.6 molar composition ($y_{CH_4}$), typical of biogas composition and some natural gas sources, the composition in the adsorbed phase ($x_{CH_4}$) is 0.015 on Chit_sup$CO_2$, 0.027 on Chit-PMO/$H_2SO_4$_P800_crushed, 0.032 at Chit-PMO/$H_2SO_4$_P800, 0.037 on Chit-PMO _crushed and 0.078 on Chit-PMO at 500 kPa and 25 °C. This means that the adsorbed phase is richer in carbon dioxide than in methane for all materials. Chit_sup$CO_2$_P800 adsorbs almost pure carbon dioxide (0.985 molar composition) under these conditions. Complete phase diagrams were also obtained (Figure S6), which confirm the excellent performance of the Chit_sup$CO_2$_P800 adsorbent, both in terms of selectivity and adsorption capacity.

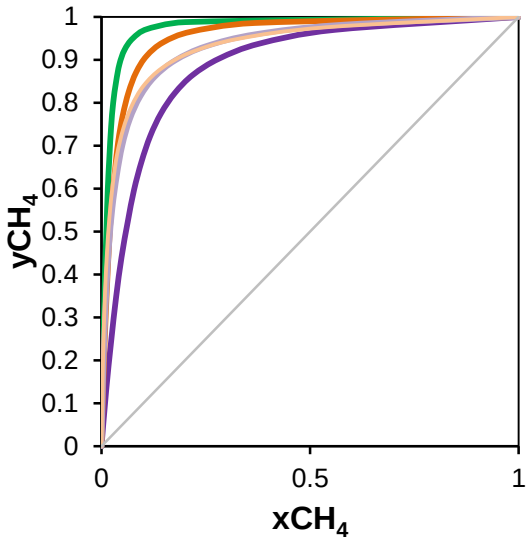


**Figure 6.** Isothermal (25 °C), isobaric (500 kPa) *xy* diagrams of $CO_2/CH_4$ mixture on the Chit_sup$CO_2$_P800 and Chit-PMO_P800 based materials. $y_{CH_4}$ and $x_{CH_4}$ are the molar fractions of methane in the gas and in the adsorbed phases, respectively. Scheme color: green - Chit_sup$CO_2$_P800, dark purple - Chit-PMO_P800, light purple - Chit-PMO_P800_crushed, dark orange - Chit-PMO_P800/$H_2SO_4$_P800 and light orange - Chit-PMO_P800/$H_2SO_4$_P800_crushed.

The viability of adsorbent materials for industrial applications on the separation of gases can be evaluated only if the material can be easily regenerated with minimum loss of capacity after each regeneration cycle. A first assessment of the regeneration of Chit_sup$CO_2$_P800 is done using just vacuum during half hour at ambient temperature (25 °C). This corresponds to what can happen industrially during the regeneration step of a vacuum swing adsorption process (VSA).[41] Figure 7 shows that the Chit_sup$CO_2$_P800 adsorbent maintained the adsorption capacity for $CO_2$ at least up to three adsorption-desorption cycles. This indicates the easy regeneration of the adsorbent and its stability to be used under cyclic separation processes. Nevertheless, for an industrial application a higher number of cycles are needed to confirm the stability.

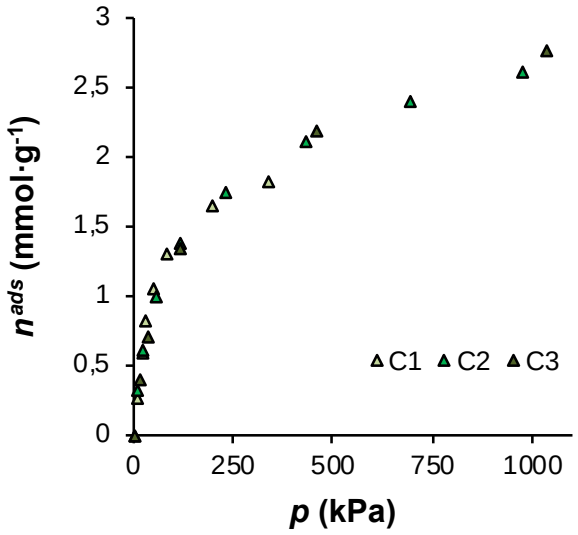


**Figure 7.** Adsorption capacity of Chit_sup$CO_2$_P800 on three $CO_2$ adsorption cycles (C1- 1st run, C2- 2nd run and C3- 3rd run).

### 3.3. Comparison to other materials

The capacity of pyrolyzed chitosan and pyrolyzed chitosan-PMO -based materials to capture carbon dioxide and methane is compared in Table 3 with the capacities reported in the literature (references provided in Table 3) for other classes of adsorbents, namely carbons, clays, MOFs, silicas, zeolites and zeolitic imidazolate framework (ZIFs) and PMOs. The values of the adsorption capacity and the $CO_2/CH_4$ capacity ratio for each material are obtained from measurements acquired at 100 kPa of pressure. Therefore, it must be emphasized that the data was determined at different temperatures, presenting the associated effects on the values of the adsorption capacities. For example, the microwave activated carbon (MAC) material[17] shows a 20% reduction in the $CO_2$ capacity when the temperature is increased from 25 to 35 °C. Nevertheless, the $CO_2/CH_4$ adsorption ratio is almost unchanged in this case, as the adsorption capacity for the $CH_4$ is also reduced in 20%.[17]

**Table 3.** Capacities of different adsorbents in the $CO_2$ / $CH_4$ separation at 100 kPa.

| Type | Materials | $CO_2$ capacity ($mol \cdot kg^{-1}$) | $CH_4$ capacity ($mol \cdot kg^{-1}$) | Temperature (°C) | $CO_2/CH_4$ Ratio |
|---|---|---|---|---|---|
| Carbons | MAC[17] | 2.13 | 0.98 | 25 | 2.2 |
| | | 1.69 | 0.81 | 35 | 2.1 |
| | Activated Carbon[57] | ≈2.10 | ≈0.90 | | 2.3 |
| | Activated Carbon[18] | ≈1.90 | ≈1.00 | 30 | 1.9 |
| | Activated Carbon[16] | ≈2.00 | ≈1.70 | | 1.2 |
| Clays | PILC $Al_w$[42] | ≈0.40 | ≈0.07 | | 5.7 |
| | PILC $Al_B$[42] | ≈0.40 | ≈0.08 | | 5.0 |
| MOFs | MOF-14(Cu)[58] | ≈2.50 | ≈1.00 | 25 | 2.5 |
| | CPO-27-Ni[59] | ≈7.50 | ≈4.38 | | 1.7 |
| | CPO-27-Mg[59] | ≈8.75 | ≈4.29 | | 2.0 |
| | ZIF-7[4] | 2.34 | 0.13 | | 18.0 |
| | amino-MIL-53(Al)[19] | 1.96 | ≈0.30 | 30 | 6.5 |
| Silicas | a-MCMBs[60] | 1.97 | 1.23 | 25 | 1.6 |
| | APTES@SBA-15[24] | ≈1.29 | ≈0.44 | | 2.9 |
| | APTES@STMB[24] | ≈1.48 | ≈0.38 | | 3.9 |
| | APTES@SHEPF[24] | ≈2.39 | ≈0.31 | | 7.7 |
| | APTES@STMBF[24] | ≈1.87 | ≈0.06 | | 31.2 |
| | MCM-41[61] | ≈0.70 | ≈0.16 | | 4.4 |
| | ASMS-3A[62] | 0.80 | 0.08 | 10 | 10.0 |
| | ASMS-5A[62] | 0.73 | 0.01 | | 73.0 |
| | N-3@SBA-15[25] | ≈1.39 | ≈0.01 | 25 | 139.0 |
| Zeolites and ZIFs | Hβ-zeolite[63] | 1.76 | 0.38 | 30 | 4.6 |
| | Naβ-zeolite[63] | ≈2.80 | ≈0.70 | | 4.0 |
| | T-type zeolite[64] | ≈1.90 | ≈0.30 | 35 | 6.3 |
| | LiX zeolite[57] | ≈3.90 | ≈0.69 | | 5.7 |
| | 13X zeolite[65] | ≈4.08 | ≈0.50 | | 8.2 |
| | Chabazite zeolite ($r_2$KCHA)[66] | ≈3.70 | ≈1.10 | | 3.4 |
| | Zeolite[18] | ≈3.70 | ≈0.60 | 30 | 6.1 |
| PMOs | $PhC_{18}$PMO[67] | 0.49 | 0.11 | 25 | 4.5 |
| | $PhC_{12}$PMO[22] | 0.37 | 0.08 | | 4.6 |
| | $NH_2PhC_{12}$PMO[22] | 0.40 | 0.07 | | 5.7 |
| | APTMS@$PhC_{12}$PMO[22] | 0.72 | 0.07 | | 10.3 |
| | APTMS@$NH_2PhC_{12}$PMO[22] | 0.50 | 0.06 | | 8.3 |
| | $PhC_{12}$PMO_P800[32] | 0.65 | 0.18 | | 3.6 |
| | $BphC_{18}$PMO_P1200[32] | 0.93 | 0.17 | | 5.5 |
| Graphitic Carbons | NAPC1-6[68] | 3.8 | 1.0 | | 3.8 |
| | NAPC2-6[68] | 3.9 | 1.3 | | 3.0 |
| | SNMC-2-600[69] | 4.24 | 1.57 | | 2.7 |
| | Chit_sup$CO_2$_P800 (this study) | ≈1.37 | ≈0.01 | | 137.0 |
| | Chit-PMO_P800 (this study) | ≈0.30 | ≈0.01 | | 30.0 |
| | Chit-PMO_P800/$H_2SO_4$_P800 (this study) | ≈0.58 | ≈0.02 | | 29.0 |
| | Chit-PMO_P800_crushed (this study) | ≈1.01 | ≈0.14 | | 7.2 |

The data in Table 3 shows that the capacity of the Chit_sup$CO_2$_P800 material to adsorb $CO_2$ (1.37 mmol·$g^{-1}$) is superior to those obtained for PMOs and clays, but it is still lower than those obtained for activated carbons, zeolites and MOFs. Interestingly, however, the Chit_sup$CO_2$ adsorbent revealed one of the lowest adsorption capacity for $CH_4$ (≈0.01 mmol·$g^{-1}$) which is only observed before for the amorphous silica (ASMS-5A), revealing one of the highest values of $CO_2/CH_4$ capacity ratio (137.0) of the materials compared and making it very convenient for separation processes. The most selective material in Table 3 for the $CO_2/CH_4$ separation is the amine functionalized silica (N-3@SBA-15) that presents similar $CO_2$ adsorption capacity (1.39 mmol·$g^{-1}$) than Chit_sup$CO_2$_P800 adsorbent. Considerably below follows the APTES@STMBF material presenting ca. 4 times lower $CO_2/CH_4$ ratio than Chit_sup$CO_2$_P800 adsorbent. We must recall that the preparation of N-3@SBA-15 and APTES@STMBF requires amine silica functionalization. The preparation of mesoporous silicas and its functionalization is not ecofriendly since the reactants are not obtained from renewable resources and the procedures use expensive noxious reactants and solvents. In fact, this is also the case for most MOFs, zeolites and PMOs. On the contrary, the Chit_sup$CO_2$_P800 is prepared with a water-based synthesis using as raw material chitosan – a biopolymer obtained from waste products. Thus Chit_sup$CO_2$ is an excellent adsorbent to be considered for large scale production and application in industrial $CO_2/CH_4$ adsorption/separation processes, combining an exceptional selectivity with an easy preparation methodology from low cost renewable raw materials.

## 4. Conclusions

Pyrolyzed chitosan and pyrolyzed chitosan-PMO materials were successfully prepared with different surface areas, pore sizes and nitrogen content. All materials are tested in the $CO_2$ and $CH_4$ adsorption (Figure 4). The adsorption of $CO_2$ is much higher than that of $CH_4$, anticipating high $CO_2$ selectivity. The use of supercritical $CO_2$ to dry the chitosan spheres is revealed to be the most interesting drying methodology. These superior properties of the supercritical $CO_2$ dried sample are certainly a consequence of the several N species, observed by XPS (Figure 3), which can interact strongly with $CO_2$. The addition of the phenylene-PMO material during the preparation of the chitosan-PMO particles leads to an increase of the specific surface area, but also to a reduction of the N content in the final material, finally not leading to selectivity improvements. Nevertheless, it is observed that the activation with sulfuric acid opens the surface of the pyrolyzed chitosan-PMO particles for the $CO_2$ molecules leading to an improvement in the $CO_2$ adsorption capacity and selectivity for the $CO_2/CH_4$ separation.

Specifically, the adsorbent with the best physical and chemical features to adsorb $CO_2$ is the Chit_sup$CO_2$ material, with a very high affinity for $CO_2$ (Henry's constant of $7.73 \times 10^{-2}$ $mol \cdot kg^{-1} \cdot kPa^{-1}$) and an extremely low affinity for $CH_4$ (Henry's constant of $0.02 \times 10^{-2}$ $mol \cdot kg^{-1} \cdot kPa^{-1}$). This material showing the highest selectivity value (95 at 500 kPa, Figure 5) in the $CO_2/CH_4$ separation and adsorbing almost pure carbon dioxide (0.99 molar composition, Figure 6) under these conditions over a wide range of gas compositions, can be easily regenerated in adsorption-desorption cycles only by exertion of vacuum (Figure 7). This indicates the possible regeneration of the Chit_sup$CO_2$_P800 that together with its simple preparation from a renewable raw material using a simple preparation method are crucial factors for its potential application in cyclic separation processes.

**Associated content**

Supplementary material (SM) is available. It includes all details and data of -196 °C $N_2$-sorption isotherms, SEM, EA, FTIR spectra, Raman spectra, and pure $CO_2$ and $CH_4$ phase diagrams at 25 °C and 500 kPa for all prepared materials.

**Notes**

The authors declare no competing financial interest.

**Acknowledgments**

This work was developed in the scope of the projects CICECO-Aveiro Institute of Materials POCI-01-0145-FEDER-007679 (Ref. FCT UID/CTM/50011/2013) and CERENA (Ref. FCT UID/ECI/04028/2013), IF/00993/2012/CP0172/CT0013 and in part, in the scope of the Smart Green Homes Project POCI-01-0247-FEDER-007678, a co-promotion between Bosch Termotecnologia S.A. and the University of Aveiro. These projects are financed by Portugal 2020 under the Competitiveness and Internationalization Operational Program and by the European Regional Development Fund (FEDER). The authors are thankful to Carlos M. Silva and Marcelo M. R. Melo for the help in drying the chitosan-based spheres with supercritical $CO_2$, to Rosana Pinto for the determination of $N_2$-sorption isotherms and to Fundação para a Ciência e a Tecnologia (FCT) for the Investigator FCT program (PC, MLP and JRBG) and the grant ref. SFRH/BD/80883/2011 (MAOL) and SFRH/BPD/100627/2014 (CN).

**References**

[1] M. Harasimowicz, P. Orluk, G. Zakrzewska-Trznadel, A.G. Chmielewski, Application of polyimide membranes for biogas purification and enrichment., J. Hazard. Mater. 144 (2007) 698–702. doi:10.1016/j.jhazmat.2007.01.098.

[2] E. Favre, R. Bounaceur, D. Roizard, Biogas, membranes and carbon dioxide capture, J. Memb. Sci. 328 (2009) 11–14. doi:10.1016/j.memsci.2008.12.017.

[3] S. Heile, S. Rosenberger, A. Parker, B. Jefferson, E.J. McAdam, Establishing the suitability of symmetric ultrathin wall polydimethylsiloxane hollow-fibre membrane contactors for enhanced $CO_2$ separation during biogas upgrading, J. Memb. Sci. 452 (2014) 37–45. doi:10.1016/j.memsci.2013.10.007.

[4] X. Wu, M. Niknam Shahrak, B. Yuan, S. Deng, Synthesis and characterization of zeolitic imidazolate framework ZIF-7 for $CO_2$ and $CH_4$ separation, Microporous Mesoporous Mater. 190 (2014) 189–196. doi:10.1016/j.micromeso.2014.02.016.

[5] P.K. Sahoo, M. John, B.L. Newalkar, N.V. Choudhary, K.G. Ayappa, Filling characteristics for an activated carbon based adsorbed natural gas storage system, Ind. Eng. Chem. Res. 50 (2011) 13000–13011. doi:dx.doi.org/10.1021/ie200241x.

[6] S.J. Bhadra, S. Farooq, Separation of methane–nitrogen mixture by pressure swing Adsorption for Natural Gas Upgrading, Ind. Eng. Chem. Res. 50 (2011) 14030–14045.

[7] P. Jaramillo, H.S. Matthews, Landfill-Gas-to-Energy Projects: Analysis of Net Private and Social Benefits, Environ. Sci. Technol. 39 (2005) 7365–7373.

[8] I. Dimitriou, P. García-Gutiérrez, R.H. Elder, R.M. Cuéllar-Franca, A. Azapagic, R.W.K. Allen, Carbon dioxide utilisation for production of transport fuels: Process and economic analysis, Energy Environ. Sci. 8 (2015) 1775–1789. doi:10.1039/c4ee04117h.

[9] B.P. Spigarelli, S.K. Kawatra, Opportunities and challenges in carbon dioxide capture, J. $CO_2$ Util. 1 (2013) 69–87. doi:10.1016/j.jcou.2013.03.002.

[10] S. Cavenati, C.A. Grande, A.E. Rodrigues, Removal of carbon dioxide from natural gas by vacuum swing adsorption, Energy Fuels. 20 (2006) 2648–2659. doi: 10.1021/ef060119e

[11] Y.S. Bae, R.Q. Snurr, Development and evaluation of porous materials for carbon dioxide separation and capture, Angew. Chemie. 50 (2011) 11586–11596. doi: 10.1002/anie.201101891

[12] E.J. García, J. Pe, G.D. Pirngruber, C. Jallut, M. Palomino, F. Rey, S. Valencia, Tuning the adsorption properties of zeolites as adsorbents for $CO_2$ separation : Best compromise between the working capacity and selectivity, Ind. Eng. Chem. Res. 53 (2014) 9860–9874. doi:10.1021/ie500207s.

[13] C. Moreno-Castilla, M.A. Ferro-García, J.P. Joly, I. Bautista-Toledo, F. Carrasco-Marín, J. Rivera-Utrilla, Activated carbon surface modifications by nitric acid, hydrogen peroxide, and ammonium peroxydisulfate treatments, Langmuir. 11 (1995) 4386–4392. doi:10.1021/la00011a035.

[14] A. Arenillas, K.M. Smith, T.C. Drage, C.E. Snape, $CO_2$ capture using some fly ash-derived carbon materials, Fuel. 84 (2005) 2204–2210. doi:10.1016/j.fuel.2005.04.003.

[15] N.P. Wickramaratne, M. Jaroniec, Activated carbon spheres for $CO_2$ adsorption, ACS Appl Mater Interfaces. 5 (2013) 1849–1855. doi:10.1021/am400112m.

[16] S. Khalili, B. Khoshandam, M. Jahanshahi, A comparative study of $CO_2$ and $CH_4$ adsorption using activated carbon prepared from pine cone by phosphoric acid activation, Korean J. Chem. Eng. 33 (2016) 2943–2952. doi:10.1007/s11814-016-

0138-y.

[17] H. Yi, F. Li, P. Ning, X. Tang, J. Peng, Y. Li, H. Deng, Adsorption separation of $CO_2$, $CH_4$, and $N_2$ on microwave activated carbon, Chem. Eng. J. 215–216 (2013) 635–642. doi:10.1016/j.cej.2012.11.050.

[18] F.V.S. Lopes, C.A. Grande, A.M. Ribeiro, J.M. Loureiro, O. Evaggelos, V. Nikolakis, A.E. Rodrigues, Adsorption of $H_2$, $CO_2$, $CH_4$, CO, $N_2$ and $H_2O$ in activated carbon and zeolite for hydrogen production, Sep. Sci. Technol. 44 (2009) 1045–1073. doi:10.1080/01496390902729130.

[19] S.A. Peter, G. V. Baron, J. Gascon, F. Kapteijn, J.F.M. Denayer, Dynamic desorption of $CO_2$ and $CH_4$ from amino-MIL-53(Al) adsorbent, Adsorption. 19 (2013) 1235–1244. doi:10.1007/s10450-013-9564-x.

[20] M.A.O. Lourenço, J.R.B. Gomes, P. Ferreira, Gas-organic and gas-inorganic interfacial effects in gas / adsorbent interactions: The case of $CO_2$/$CH_4$ separation, in: M.-H. Delville, A. Taubert (Eds.), Hybrid organic-inorganic interfaces towards advanced Functional Materials, 1st ed., Wiley-VCH Verlag GmbH & Co. KGaA, 2018: pp. 413–458. doi:10.1002/9783527807130.ch9.

[21] M. Keramati, A.A. Ghoreyshi, Improving $CO_2$ adsorption onto activated carbon through functionalization by chitosan and triethylenetetramine, Phys. E Low-Dimensional Syst. Nanostructures. 57 (2014) 161–168. doi:10.1016/j.physe.2013.10.024.

[22] M.A.O. Lourenço, C. Siquet, M. Sardo, J. Pires, L. Mafra, M. Jorge, M.L. Pinto, P. Ferreira, J. Pires, M. Jorge, M.L. Pinto, P. Ferreira, J.R.B. Gomes, Interaction of $CO_2$ and $CH_4$ with functionalized periodic mesoporous phenylene–silica: Periodic DFT calculations and gas adsorption measurements, J. Phys. Chem. C. 120 (2016) 3863–

3875. doi:10.1021/acs.jpcc.5b11844.

[23] M.A.O. Lourenço, C. Siquet, J.C. Santos, M. Jorge, J.R.B. Gomes, P. Ferreira, Insights into $CO_2$ and $CH_4$ Adsorption by Pristine and Aromatic Amine-Modified Periodic Mesoporous Phenylene-Silicas, J. Phys. Chem. C. 120 (2016) 14236–14245. doi:10.1021/acs.jpcc.6b04605.

[24] E. Vilarrasa-García, J.A. Cecilia, M. Bastos-Neto, C.L. Cavalcante, D.C.S. Azevedo, E. Rodriguez-Castellón, $CO_2/CH_4$ adsorption separation process using pore expanded mesoporous silicas functionalizated by APTES grafting, Adsorption. 21 (2015) 565–575. doi:10.1007/s10450-015-9700-x.

[25] L. Mafra, T. Čendak, S. Schneider, P. V. Wiper, J. Pires, J.R.B. Gomes, M.L. Pinto, Amine functionalized porous silica for $CO_2$/CH4 separation by adsorption: Which amine and why, Chem. Eng. J. 336 (2018) 612–621. doi:10.1016/j.cej.2017.12.061.

[26] H. Xie, S. Zhang, S. Li, Chitin and chitosan dissolved in ionic liquids as reversible sorbents of $CO_2$, Green Chem. 8 (2006) 630–633. doi:10.1039/b517297g.

[27] M.E. Boot-Handford, J.C. Abanades, E.J. Anthony, M.J. Blunt, S. Brandani, N. Mac Dowell, J.R. Fernandez, M.-C. Ferrari, R. Gross, J.P. Hallett, R.S. Haszeldine, P. Heptonstall, A. Lyngfelt, Z. Makuch, E. Mangano, R.T.J. Porter, M. Pourkashanian, G.T. Rochelle, N. Shah, J.G. Yaoa, P.S. Fennell, Carbon capture and storage update, Energy Enviromintal Sci. 7 (2014) 130–189. doi:10.1039/c3ee42350f.

[28] Z.-Z. Yang, L.-N. He, J. Gao, A.-H. Liu, B. Yu, Carbon dioxide utilization with C–N bond formation: carbon dioxide capture and subsequent conversion, Energy Environ. Sci. 5 (2012) 6602. doi:10.1039/c2ee02774g.

[29] A.K. Qaroush, K.I. Assaf, S.K. Bardaweel, A. Al-Khateeb, F. Alsoubani, E. Al-Ramahi, M. Masri, T. Brück, C. Troll, B. Rieger, A.F. Eftaiha, Chemisorption of

$CO_2$ by chitosan oligosaccharide/DMSO: Organic carbamato-carbonato bond formation, Green Chem. 19 (2017) 4305–4314. doi:10.1039/c7gc01830d.

[30] A. Primo, A. Forneli, A. Corma, H. García, From biomass wastes to highly efficient $CO_2$ adsorbents: graphitisation of chitosan and alginate biopolymers., ChemSusChem. 5 (2012) 2207–14. doi:10.1002/cssc.201200366.

[31] M. Oschatz, M. Antonietti, A search for selectivity to enable $CO_2$ capture with porous adsorbents, Energy Environ. Sci. 11 (2018) 57–70. doi:10.1039/c7ee02110k.

[32] M.A.O. Lourenço, M.L. Pinto, J. Pires, J.R.B. Gomes, P. Ferreira, Carbonization of periodic mesoporous phenylene- and biphenylene-silicas for $CO_2/CH_4$ separation, Carbon 119 (2017) 267–277.

[33] R.J.P. Corriu, J.J.E. Morea, P. Thepot, M.W. Chi Man, New mixed organic-inorganic polymers: hydrolysis and polycondensation of bis(trimethoxysilyl) organometallic precursors, Chem. Mater. 4 (1992) 1217–1224. doi: 10.1021/cm00024a020

[34] S. Inagaki, S. Guan, T. Ohsuna, O. Terasaki, An ordered mesoporous organosilica hybrid material with a crystal-like wall structure, Nature. 416 (2002) 304–307. doi:10.1038/416304a.

[35] N. Bion, P. Ferreira, A. Valente, I.S. Gonçalves, J. Rocha, Ordered benzene-silica hybrids with molecular-scale periodicity in the walls and different mesopore sizes, J. Mater. Chem. 13 (2003) 1910–1913. doi:10.1039/b304430k.

[36] T. Asefa, M.J. MacLachlan, N. Coombs, G.A. Ozin, Periodic mesoporous organosilicas with organic groups inside the channel walls, Nature. 402 (1999) 867–871. doi:10.1038/47229.

[37] S. Inagaki, S. Guan, Y. Fukushima, T. Ohsuna, O. Terasaki, Novel Mesoporous

Materials with a Uniform Distribution of Organic Groups and Inorganic Oxide in Their Frameworks, J. Am. Chem. Soc. 121 (1999) 9611–9614. doi:10.1021/ja9916658.

[38] B.J. Melde, B.T. Holland, C.F. Blanford, A. Stein, Mesoporous sieves with unified hybrid inorganic/organic frameworks, Chem. Mater. 11 (1999) 3302–3308. doi:10.1021/cm9903935.

[39] C. Nunes, É. Maricato, Â. Cunha, A. Nunes, J. A. L. da Silva, M. A. Coimbra, Chitosan-caffeic acid-genipin films presenting enhanced antioxidant activity and stability in acidic media., Carbohydr. Polym. 91 (2013) 236–43. doi:10.1016/j.carbpol.2012.08.033.

[40] A.L. Myers, Equation of state for adsorption of gases and their mixtures in porous materials, Adsorption. 9 (2003) 9–16. doi: 10.1023/A:1023807128914

[41] M.L. Pinto, J. Pires, J. Rocha, Porous materials prepared from clays for the upgrade of landfill gas, J. Phys. Chem. C. 112 (2008) 14394–14402. doi: 10.1021/jp803015d

[42] J. Pires, V.K. Saini, M.L. Pinto, Studies on selective adsorption of biogas components on pillared clays : Approach for biogas improvement, Environ. Sci. Technol. 42 (2008) 8727–8732. doi:10.1021/es8014666.

[43] K.S.W. Sing, D.H. Everett, R.A.W. Haul, L. Moscou, R.A. Pierotti, J. Rouquerol, T. Siemieniewaska, Reporting physisorption data for gas/solid systems with special reference to the determination of surface area and porosity, Pure Appl. Chem. 57 (1985) 603–619. doi:10.1351/pac198557040603.

[44] M. Thommes, K. Kaneko, A. V. Neimark, J.P. Olivier, F. Rodriguez-Reinoso, J. Rouquerol, K.S.W. Sing, Physisorption of gases, with special reference to the evaluation of surface area and pore size distribution (IUPAC Technical Report), Pure

Appl. Chem. 89 (2015) 1051–1069. doi:10.1515/pac-2014-1117.

[45] M. Robitzer, A. Tourrette, R. Horga, R. Valentin, M. Boissière, J.M. Devoisselle, F. Di Renzo, F. Quignard, Nitrogen sorption as a tool for the characterisation of polysaccharide aerogels, Carbohydr. Polym. 85 (2011) 44–53. doi:10.1016/j.carbpol.2011.01.040.

[46] S. Cardea, A. Gugliuzza, M. Sessa, M.C. Aceto, E. Drioli, E. Reverchon, Supercritical gel drying : A powerful tool for tailoring symmetric porous PVDF-HFP membranes, ACS Appl. Mater. Interfaces. 1 (2009) 171–180. doi:10.1021/am800101a.

[47] J. Zawadzki, H. Kaczmarek, Thermal treatment of chitosan in various conditions, Carbohydr. Polym. 80 (2010) 394–400. doi:10.1016/j.carbpol.2009.11.037.

[48] H. Kaczmarek, J. Zawadzki, Chitosan pyrolysis and adsorption properties of chitosan and its carbonizate, Carbohydr. Res. 345 (2010) 941–947. doi:10.1016/j.carres.2010.02.024.

[49] G.N. Kalantzopoulos, A. Enotiadis, E. Maccallini, M. Antoniou, K. Dimos, A. Policicchio, E. Klontzas, E. Tylianakis, V. Binas, P.N. Trikalitis, R.G. Agostino, D. Gournis, G.E. Froudakis, Hydrogen storage in ordered and disordered phenylene-bridged mesoporous organosilicas, Int. J. Hydrogen Energy. 39 (2014) 2104–2114. doi: 10.1016/j.ijhydene.2013.11.063

[50] S. Biniak, A. Świątkowski, M. Pakuła, Electrochemical studies of phenomena at active carbon-electrolyte solution interfaces, in: Ljubisa R. Radovic (Ed.) Chemistry and physics of carbon: A series of advances, Marcel Dekker, Inc., New York, 2001: pp. 126–224. ISBN 9780824702465 - CAT# DK1545

[51] A.C. Ferrari, J. Robertson, Resonant Raman spectroscopy of disordered, amorphous,

and diamondlike carbon, Phys. Rev. B - Condens. Matter Mater. Phys. 64 (2001) 1–13. doi:10.1103/PhysRevB.64.075414.

[52] M.A. Tamor, W.C. Vassell, Raman "fingerprinting" of amorphous carbon films, J. Appl. Phys. 76 (1994) 3823–3830. doi:10.1063/1.357385.

[53] N.P. Wickramaratne, J. Xu, M. Wang, L. Zhu, L. Dai, M. Jaroniec, Nitrogen enriched porous carbon spheres: Attractive materials for supercapacitor electrodes and $CO_2$ adsorption, Chem. Mater. 26 (2014) 2820–2828. doi:10.1021/cm5001895.

[54] F. Cataldo, A study on the thermal stability to 1000°C of various carbon allotropes and carbonaceous matter both under nitrogen and in air, Fullerenes Nanotub. Carbon Nanostructures. 10 (2002) 293–311. doi:10.1081/FST-120016451.

[55] A.L. Myers, J.M. Prausnitz, Thermodynamics of mixed-gas adsorption, AIChE J. 11 (1965) 121–127. doi:10.1002/aic.690110125.

[56] R.T. Yang, Gas Separation by Adsorption Processes, Butterworths Publishers: Boston, 1987. doi:10.1016/B978-0-409-90004-0.50001-5.

[57] Y. Park, D.-K. Moon, Y.-H. Kim, H. Ahn, C.-H. Lee, Adsorption isotherms of $CO_2$, CO, $N_2$, $CH_4$, Ar and $H_2$ on activated carbon and zeolite LiX up to 1.0 MPa, Adsorption. 20 (2014) 631–647. doi:10.1007/s10450-014-9608-x.

[58] J.R. Karra, B.E. Grabicka, Y.-G. Huang, K.S. Walton, Adsorption study of $CO_2$, $CH_4$, $N_2$, and $H_2O$ on an interwoven copper carboxylate metal-organic framework (MOF-14)., J. Colloid Interface Sci. 392 (2013) 331–336. doi:10.1016/j.jcis.2012.10.018.

[59] P.D.C. Dietzel, V. Besikiotis, R. Blom, Application of metal–organic frameworks with coordinatively unsaturated metal sites in storage and separation of methane and

carbon dioxide, J. Mater. Chem. 19 (2009) 7362–7370. doi:10.1039/b911242a.

[60] X. Peng, W. Wang, R. Xue, Z. Shen, Adsorption separation of $CH_4/CO_2$ on mesocarbon microbeads: Experiment and modeling, AIChE J. 52 (2006) 994–1003. doi:10.1002/aic.10723.

[61] Y. Belmabkhout, A. Sayari, Adsorption of $CO_2$ from dry gases on MCM-41 silica at ambient temperature and high pressure. 2: Adsorption of $CO_2/N_2$, $CO_2/CH_4$ and $CO_2/H_2$ binary mixtures, Chem. Eng. Sci. 64 (2009) 3729–3735. doi:10.1016/j.ces.2009.05.039.

[62] K. Morishige, Adsorption and separation of $CO_2/CH_4$ on amorphous silica molecular sieve, Science 115 (2011) 9713–9718. doi:10.1021/jp202572w.

[63] X. Xu, X. Zhao, L. Sun, X. Liu, Adsorption separation of carbon dioxide, methane, and nitrogen on Hβ and Na-exchanged β-zeolite, J. Nat. Gas Chem. 17 (2008) 391–396. doi:10.1016/S1003-9953(09)60015-3.

[64] M.D. Rad, S. Fatemi, S.M. Mirfendereski, Development of T type zeolite for separation of $CO_2$ from $CH_4$ in adsorption processes, Chem. Eng. Res. Des. 90 (2012) 1687–1695. doi:10.1016/j.cherd.2012.01.010.

[65] S. Cavenati, C.A. Grande, A.E. Rodrigues, Adsorption equilibrium of methane, carbon dioxide, and nitrogen on zeolite 13X at high pressures, J. Chem. Eng. Data. 49 (2004) 1095–1101. doi:10.1021/je0498917.

[66] J. Shang, G. Li, R. Singh, Q. Gu, K.M. Nairn, T.J. Bastow, N. Medhekar, C.M. Doherty, A.J. Hill, J.Z. Liu, P.A. Webley, Discriminative separation of gases by a "molecular trapdoor" mechanism in chabazite zeolites, J. Am. Chem. Soc. 134 (2012) 19246–19253. doi:10.1021/ja309274y.

[67] M.A.O. Lourenço, R.M. Silva, R.F. Silva, N. Pinna, S. Pronier, J. Pires, J.R.B.

Gomes, M.L. Pinto, P. Ferreira, Turning periodic mesoporous organosilicas selective to $CO_2/CH_4$ separation: deposition of aluminium oxide by atomic layer deposition, J. Mater. Chem. A. 3 (2015) 22860–22867. doi:10.1039/C5TA05964J.

[68] J. Wang, P. Zhang, L. Liu, Y. Zhang, J. Yang, Z. Zeng, S. Deng, Controllable synthesis of bifunctional porous carbon for efficient gas-mixture separation and high-performance supercapacitor, Chem. Eng. J. 348 (2018) 57–66. doi:10.1016/j.cej.2018.04.188.

[69] P. Zhang, Y. Zhong, J. Ding, J. Wang, M. Xu, Q. Deng, Z. Zeng, S. Deng, A new choice of polymer precursor for solvent-free method: Preparation of N-enriched porous carbons for highly selective $CO_2$ capture, Chem. Eng. J. 355 (2019) 963–973. doi:10.1016/j.cej.2018.08.219.

# Graphical abstract

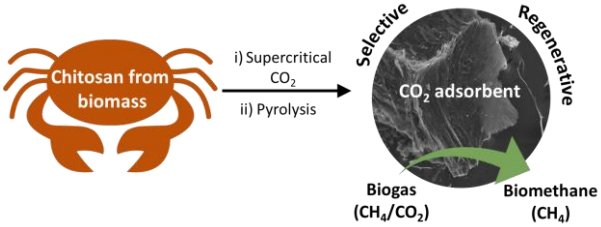

## Highlights

- Pyrolyzed chitosan-based sorbents are prepared with different structural properties;
- Materials are tested in the $CO_2/CH_4$ adsorption-separation showing $CO_2$ selectivity;
- Supercritical $CO_2$ dried samples show the best $CO_2$ adsorption and selectivity profiles;
- The best material is suitable to adsorb pure carbon dioxide.